ISSN 0021-3640, JETP Letters, 2023, Vol. 117, No. 4, pp. 276–280. © The Author(s), 2023. This article is an open access publication.
Russian Text © The Author(s), 2023, published in Pis'ma v Zhurnal Eksperimental'noi i Teoreticheskoi Fiziki, 2023, Vol. 117, No. 4, pp. 273–278.

OPTICS
AND LASER PHYSICS

On the Laser Generation in Two-Dimensional Materials with Pumping by Quasitrapped Modes

M. Yu. Gubin[a, b], A. V. Shesterikov[a, b], V. S. Volkov[b], and A. V. Prokhorov[a, b, *]

[a] *Department of Physics and Applied Mathematics, Vladimir State University, Vladimir, 600000 Russia*
[b] *Center of Photonics and Two-Dimensional Materials, Moscow Institute of Physics and Technology (National Research University), Dolgoprudnyi, Moscow region, 141701 Russia*
**e-mail: alprokhorov33@gmail.com*

Received December 23, 2022; revised January 5, 2023; accepted January 7, 2023

A model has been proposed to describe the laser generation of two-dimensional semiconductor films with near-field pumping by quasitrapped modes excited in dielectric metasurfaces. A metastructure consisting of a Si metasurface coated with a $MoTe_2$ film, where narrow-band resonance of a quasitrapped mode is joined with a broad exciton resonance of a two-dimensional material, has been designed. Threshold conditions for generation in the $MoTe_2$ film with pumping by quasitrapped modes have been determined. The possibility of polarization control of the emission of the proposed metastructure has been demonstrated.

DOI: 10.1134/S0021364023600076

The design of emitting nanodevices with pumping by a strong near field using plasmon and dielectric nanocavities is one of the significant and rapidly developed fields of modern nanophotonics. The authors of the first works [1, 2] combined exciton resonance of a quantum-confined chromophore and the near field of the plasmonic nanoparticle. However, large losses in metallic nanocavities strongly increased the threshold of laser generation. The use of nonlinear near-field and collective effects [3] only partially solves the problem of control of generation in such systems. New possibilities are based on the use of dielectric nanophotonics [4–6] to design low-threshold efficiently controlled micro- and nanolasers. In particular, positive feedback was reached in [7] by combining exciton resonance and high order Mie resonances in single perovskite nanoparticles at a low threshold of generation.

At the same time, to increase the output power of laser generation, such emitting nanoparticles can be assembled in a metasurface with the synchronization of their near field responses using collective subdiffraction effects. Synchronization can be achieved by exciting so-called photonic bound states in the continuum [8, 9], which lead to the generation of (quasi)trapped modes (QTMs) [10, 11] and to a strong concentration of the near field in the vicinity of nanoparticles and inside them. However, the excitation of a quasitrapped mode in the lattice of even weakly dissipative particles can initiate the collective enhancement of losses [12] due to the induction of strong fields inside each nanoparticle. Consequently, the metasurface can be used for the near field pumping, whereas an active medium can be photoluminescent two-dimensional semiconductor films with a thickness of one or a few atomic layers [13], in particular, transition metal dichalcogenides having record optical anisotropy [14] and bright exciton resonances [15], which are deposited on the metasurface.

The metasurface composed of Si disks with the radius R_2 and height H, each with a circular hole with the radius R_1 shifted by Δ_y along the y axis (see Fig. 1a) is used for near-field pumping. Under the irradiation of this metasurface by the linearly polarized wave $E_x(k_z)$ of the signal field, the dipole magnetic moment component m_z [12] perpendicular to the base plane can be excited in each disk owing to bianisotropy. The QTM regime [12] can be realized in the metasurface when its period T satisfies the condition of constructive interference of near-field responses of individual disks taking into account the effective permittivity of the metasurface (see Fig. 1b).

Using the strategy of search for QTMs [16], we obtain the period $T = 702$ nm for the metasurface consisting of Si disks with the parameters $R_2 = 164$ nm, $H = 110$ nm, $R_1 = 80$ nm, and $\Delta_y = 70$ nm and placed in vacuum. In this case, QTMs are excited at a wavelength of $\lambda_{QTM} = 980$ nm (see Fig. 1c). The QTM resonance in the same metasurface placed on the SiO_2 substrate is shifted to the wavelength $\lambda_{QTM} = 1050$ nm and corresponds to the reflection peak of the signal field with the full width at half maximum $w_{FWHM} = 19.7$ nm (see Fig. 1c). The quality factor of this reso-

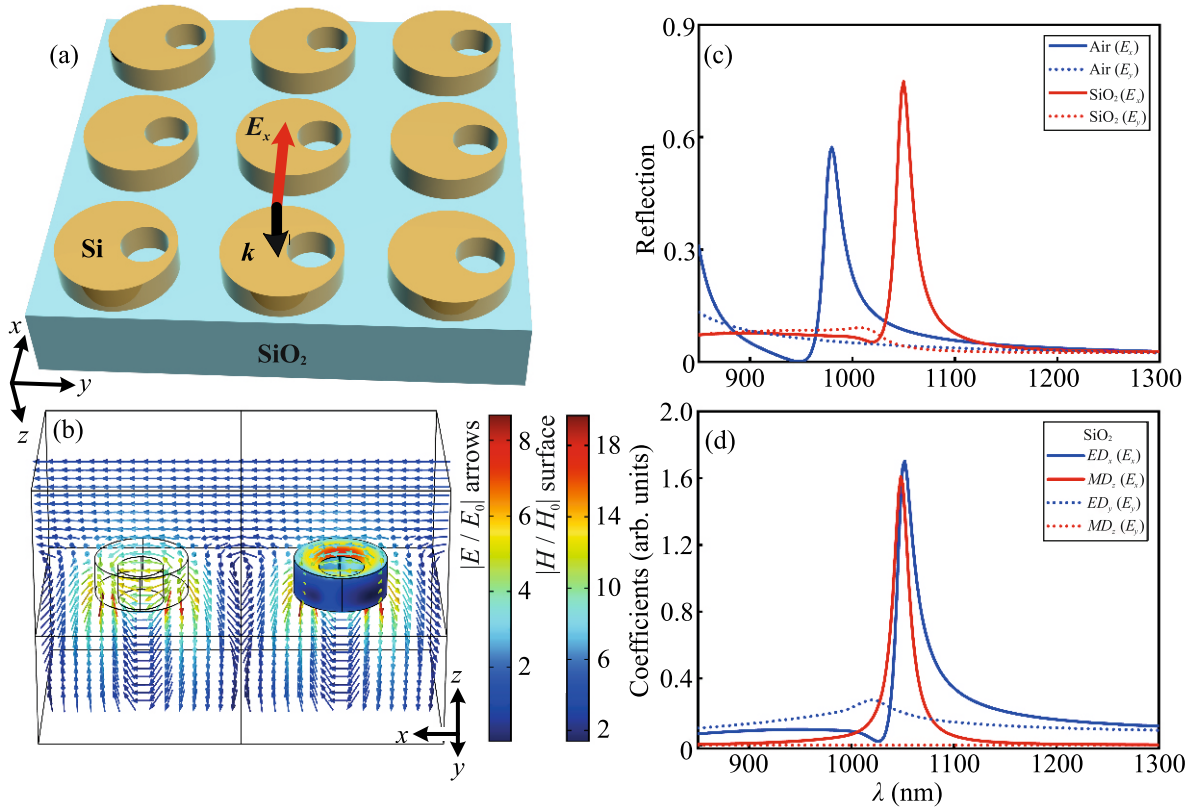

Fig. 1. (Color online) (a) Model of the metasurface of Si disks with holes. (b) Visualization of the calculated distribution of the magnetic field (indicated in color for the right disk) on the surface and the electric field (indicated by arrows) near a pair of Si disks of the metasurface in the regime of QTM excitation. (c) Reflection spectra of the metasurface placed in vacuum and on the quartz substrate, as well as at orthogonal polarizations of the signal electromagnetic wave. (d) Results of the multipole analysis for contributions from different components of the electric (ED_x for p_x and ED_y for p_y) and magnetic (MD_z for m_z) dipoles to the total scattering cross section of a single disk of the metasurface placed on the SiO_2 substrate in the regime of excitation of quasitrapped mode. The parameters of the system are $R_2 = 164$ nm, $H = 110$ nm, $R_1 = 80$ nm, $\Delta_y = 70$ nm, and $T = 702$ nm.

nance is $Q = \lambda_{QTM}/w_{FWHM} = 54$. A significant increase in the reflection coefficient of the metasurface at the QTM wavelength is due to the resonant enhancement of the emitting component p_x of the electric dipole of each disk [17, 18] (see the results of the multipole analysis in Fig. 1d). In turn, such an enhancement is due to the bianisotropic coupling between the components p_x and m_z; the latter component is responsible for the regime of QTM formation [11, 12]. The incident wave with the polarization $E_y(k_z)$ does not excite the bianisotropic component m_z in disks (Fig. 1d) because the condition of the location of the defect (hole) with respect to the polarization of the exciting field is violated [16]. As a result, the feature of the reflection coefficient of the metasurface associated with the QTM excitation disappears (see Fig. 1c). Thus, the polarizing control of both the QTM formation in the metasurface and the intensity of the near-field response for each of its building blocks becomes possible. In addition, the electric component of the near field above the surface composed of disks in the QTM regime is oriented predominantly in the plane of the metasurface (see Fig. 1b) owing to the excitation of p_x, which is a basis for the effective control of exciton resonances with the deposition of a two-dimensional film over the metasurface.

Below, we consider the $1000 \times 1000 \times 0.7$ nm flakes with a thickness of one atomic layer, which are separated from a $MoTe_2$ crystal by, e.g., the exfoliation method [19], as an active medium of the metastructure, which completely covering the metasurface. Under these conditions, $MoTe_2$ can be considered as a direct band gap semiconductor [20] with the photoluminescence wavelength λ_0 that is determined by the width of the band gap E_g and depends on the temperature. In particular, at a temperature of 4.5 K, we obtain $E_g = 1.18$ eV, $\lambda_0 = 1056$ nm [20], and the complex refractive index $\bar{n}(\lambda_0) = n(\lambda_0) + i\alpha(\lambda_0) = 4.4752 + i0.39967$ [21].

For pumping, it is possible to use a cw He–Ne laser at a wavelength of $\lambda_p = 633$ nm [13], which normally irradiates the metastructure consisting of a $MoTe_2$ monolayer film lying on the metasurface supporting QTM (see Fig. 2a). When the central wavelength λ_0 of photoluminescence of $MoTe_2$ is tuned to the wave-

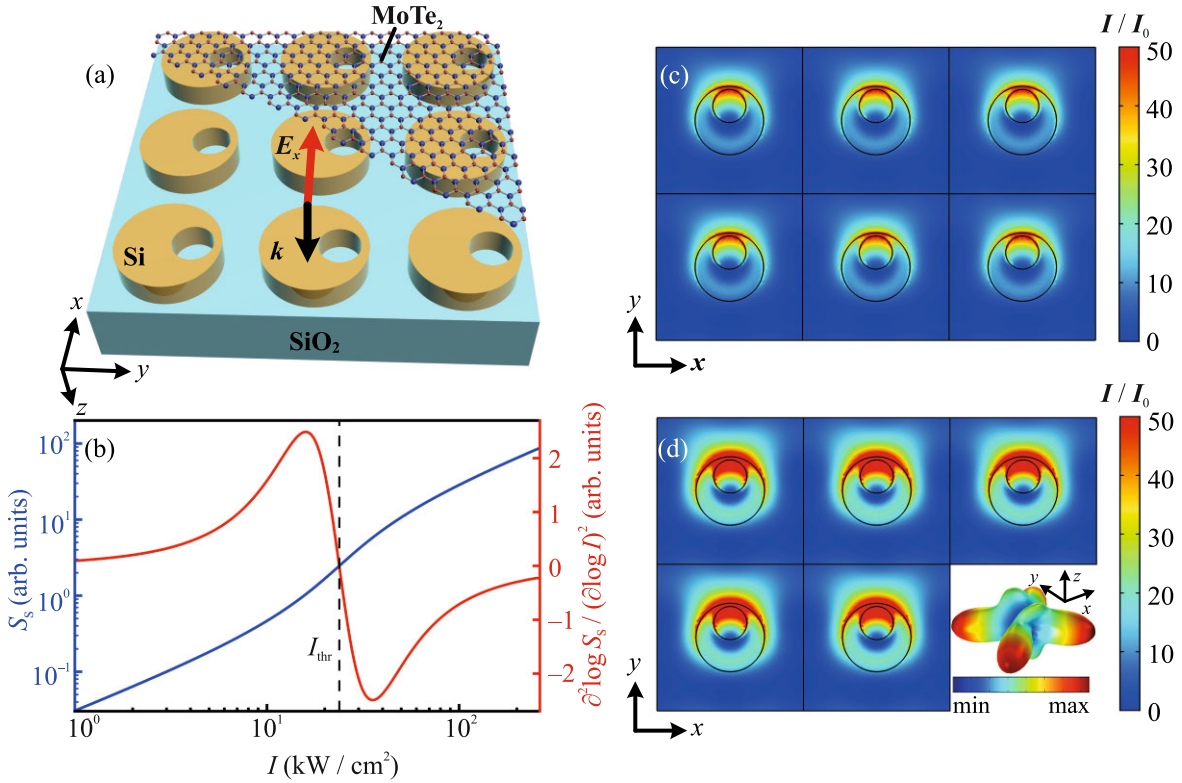

Fig. 2. (Color online) (a) Model of the metasurface in the form of thin $MoTe_2$ film deposited on the metasurface composed of Si disks with holes. (b) Steady-state photon density S_s and its derivative $\frac{d^2 \log S_s}{(d \log I)^2}$ versus the near-field pump intensity I. The dashed vertical straight line indicates the threshold of generation I_{thr}. (c, d) Visualization of the distribution of the electric field intensity in the $MoTe_2$ film over the Si metasurface in the regime of generation of quasitrapped modes in it in the (c) absence and (d) presence of the pump field with the above-threshold intensity $\overline{I} = 2.2$ kW/cm^2. The near-field intensity is given in units of the incident wave intensity. The contours of disks of the metasurface located under the $MoTe_2$ film are projected on the film by black lines. The inset in panel (d) shows the scattering pattern of one disk of the metasurface. The parameters of the Si metasurface are the same as in Fig. 1.

length λ_{QTM} of a quasitrapped mode, a significant enhancement of photoluminescence can be expected with the possibility of generation of coherent electromagnetic radiation by the system in the direction perpendicular to the plane of the metastructure. The initial optimization of the metasurface shown in Fig. 1a was performed so that the wavelength of the QTM in the metasurface coated with the $MoTe_2$ monolayer film was $\lambda_{QTM} = 1056$ nm.

Transition to the regime of generation of laser radiation can be described by rate equations for the densities of charge carriers N and photons S of the signal field [7, 22, 23] in the active $MoTe_2$ medium of the metastructure in the form

$$\frac{dN}{dt} = \frac{\alpha_p P}{\hbar\omega_p V} - R_{nr}(N) - R_{sp}(N) - \upsilon_g g(N) S, \quad (1a)$$

$$\frac{dS}{dt} = -\frac{S}{\tau_p} + \Gamma\upsilon_g g(N) S + \Gamma\beta R_{sp}(N). \quad (1b)$$

Here, $\hbar\omega_p$ is the energy of the external optical pump; α_p is the imaginary part of the refractive index for $MoTe_2$ at a pump wavelength; V is the volume of the structure; $\tau_p = Q/\omega_0$ and $\omega_0 = \frac{2\pi c}{\lambda_0}$ are the lifetime and frequency of the lasing mode, respectively; Γ is the confinement factor of the lasing mode; β is the spontaneous emission coefficient determined by the Purcell factor; P is the pump power; $R_{nr} = N/\tau_{nr} + CN^3$ and $R_{sp} = N/\tau_{sp}$ are the nonradiative recombination and total spontaneous emission rates, respectively, where τ_{nr} and τ_{sp} are the nonradiative and spontaneous recombination times, respectively, and C is the Auger recombination coefficient; $g(N) = a(N - N_{tr})$ is the active medium gain, where a is the linear gain coefficient and N_{tr} is the density of electron–hole pairs necessary for the transparency regime of the medium; and $\upsilon_g = c/n_g$ is the group velocity of generated radiation in the active medium, where c is the speed of light in vacuum, and we assume that $n_g = n(\lambda_0)$. Below, following

[24], we take $\tau_{sp} = 3$ ps (cf. 4 ps in [13]), $\tau_{nr} = 23$ ps, $C = 10^{-40}$ m^6 s^{-1} [7], $\beta = 0.1$, and $\Gamma = 0.04038$ for the $MoTe_2$ monolayer film.

The stationary solution of Eqs. (1a) and (1b) for the photon density S_s and pump power P depends on the stationary carrier density N_s and has the form [22]

$$S_s(N_s) = \frac{\beta\Gamma\tau_p N_s}{\tau_{sp}(1 + \Gamma\upsilon_g a\tau_p(N_{tr} - N_s))}, \quad (2a)$$

$$P(N_s) = \frac{\hbar\omega_p V}{\alpha_p}\left(CN_s^3 + \frac{N_s}{\tau_{nr}} + (1-\beta)\frac{N_s}{\tau_{sp}} + \frac{S_s(N_s)}{\Gamma\tau_p}\right). \quad (2b)$$

Figure 2b presents the parametric gain curves for S_s versus the pump intensity $I = P(N_s)/A_{str}$, where A_{str} is the area of the flake. In particular, the threshold of laser generation is determined as the position of the inflection point of the gain curve $S_s(I)$ on a log–log scale, which corresponds to the condition [13, 25]

$$\frac{d^2 \log S_s}{(d \log I)^2} = 0. \quad (3)$$

The complex permittivity of $MoTe_2$ under pumping at the wavelength λ_p can be represented in the form [7]

$$\varepsilon(\omega) = \varepsilon_r(\omega) + \frac{f_0\omega_0^2}{\omega_0^2 - \omega^2 - i\gamma\omega}, \quad (4)$$

where $\varepsilon_r(\omega) = \mathrm{Re}[(\bar{n}(\omega))^2]$ is the permittivity of $MoTe_2$ without pumping, i.e., when $f_0 = 0$; f_0 corresponds to the amplification amplitude at the wavelength λ_0 with the Lorentzian lineshape; and $\gamma = 1/\tau_p$. As in [26], the isotropic permittivity $\varepsilon_r(\omega) \approx \varepsilon_{\|}(\omega)$ was used for $MoTe_2$ [21] in the calculations because the electric component of the QTM is oriented predominantly along the surface of the film (see Fig. 1b).

In the numerical simulation, we varied the imaginary part of the permittivity $\varepsilon(\omega)$ of $MoTe_2$ to values at which losses were completely compensated; i.e., the reflection coefficient of the signal field from the metastructure became 1. In this case, $f_0 = \mathrm{Im}[(n(\omega_0) + ik_g)^2]\gamma/\omega_0$ and the threshold gain coefficient g_{thr} of the entire metastructure can be obtained using the expression $k_g = -\frac{g\lambda_0}{4\pi}$ [27, 28] for the imaginary part of the refractive index. For the case under consideration in Fig. 2a, the threshold conditions correspond to the effective permittivity $\varepsilon_{eff} = 2.3207 - 0.5012i$ (recalculated from the permittivity $\varepsilon = 19.8674 - 7.1603i$ of the $MoTe_2$ monolayer replacing its actual thickness by an effective one of 10 nm used in the simulation, see below) and, setting $N_{tr} = 1.61 \times 10^{17}$ cm^{-3} and $a = 7.08 \times 10^{-18}$ m^2, we obtain $k_g = -0.8$, which corresponds to $g_{thr} = 95194$ cm^{-1} and the threshold near-field pump intensity $I_{thr} = 23.78$ kW/cm^2 (with the threshold power $P_{thr} = 0.238$ mW) and occurs at the carrier density $N_{thr} = 1.51\times10^{18}$ cm^{-3}.

The near-field response of the metastructure under consideration was numerically simulated using COMSOL Multiphysics software. To simulate the $MoTe_2$ thin film with the thickness h beyond the resolution of the algorithm, we recalculated the actual permittivity $\varepsilon(\omega)$ to the effective one $\varepsilon_{eff}(\omega)$ for a thicker film with the thickness h_F similar in properties:

$$\varepsilon_{eff}(\omega) = 1 + (\varepsilon(\omega) - 1)\frac{h}{h_F}, \quad (5)$$

where $h = 0.7$ nm is the actual thickness of the $MoTe_2$ film and $h_F = 10$ nm is the effective thickness of the $MoTe_2$ film used in the numerical simulation.

Figure 2c shows the electric field inside the $MoTe_2$ film over the metasurface in the regime of QTM excitation at the wavelength $\lambda_{QTM} = 1056$ nm but in the absence of an additional pump field. The pump field increasing the intensity of the near-field response of disks to $I = 200$ kW/cm^2 results in the above-threshold conditions with the effective permittivity $\varepsilon_{eff} = 2.3207 - 0.6538i$ and the corresponding gain $k_g = -1.0435$ of the film. Since the $MoTe_2$ film is in fact pumped by the near field at "hot points" on the surface of Si disks (see Fig. 2d), the intensity of the optical pump field $\bar{I}$ in the far field region necessary to implement the lasing regime decreases by a factor of about 90. In the case under consideration, this intensity is $\bar{I} = 2.2$ kW/cm^2 (see Fig. 2d). In fact, this corresponds to a decrease in the threshold of generation to $\bar{I}_{thr} = 264$ W/cm^2.

The radiation pattern presented in the inset of Fig. 2d shows that the most part of the energy of the incident wave is concentrated and scattered in the plane of the metasurface. This incoherent process is related to the excitation of nonemitting magnetic dipole m_z in the QTM regime. In this case, only a part of the energy stored by the metasurface is reemitted owing to the bianisotropy-induced excitation of the component p_x of the electric dipole. However, this is sufficient for the excess of threshold conditions and for the formation of a coherent signal from the entire metasurface coated with the active medium. In this case, the regime of QTM excitation and generation in the system can be controlled simply by the switching of the polarization of the signal field. A much higher energy efficiency can be expected in the implementation of QTMs on the basis of electric bianisotropy with the excitation of the p_z component in each disk [16]. Semiconductor quantum dots generating coher-

ent radiation in the plane of the metasurface can serve as an active medium for such a system.

To conclude, we note that a much higher Q factor can be achieved in the presented system with pumping by QTMs [9, 16] and a decrease in the threshold of generation down to several watts per centimeter squared can be expected. Furthermore, the use of open resonator systems based on quasitrapped modes in quasi-infinite lattices makes it possible to significantly extend the dimensions of the active region and to fabricate scaled devices and metacoatings generating laser radiation. Such coatings can be placed on flexible and conducting substrates, fabricated by laser printing [29] or on the basis of liquid metamaterials [30], and controlled by an external electric field.

ACKNOWLEDGMENTS

We are deeply grateful to Prof. A.B. Evlyukhin for stimulating discussions.

FUNDING

This work was supported by the Russian Science Foundation (project no. 22-22-01020, https://rscf.ru/project/22-22-01020).

CONFLICT OF INTEREST

The authors declare that they have no conflicts of interest.

OPEN ACCESS

REFERENCES

1. M. I. Stockman, J. Opt. **12**, 024004 (2010).
2. M. A. Noginov, G. Zhu, A. M. Belgrave, R. Bakker, V. M. Shalaev, E. E. Narimanov, S. Stout, E. Herz, T. Suteewong, and U. Wiesner, Nature (London, U.K.) **460**, 1110 (2009).
3. A. V. Shesterikov, M. Yu. Gubin, S. N. Karpov, and A. V. Prokhorov, JETP Lett. **107**, 435 (2018).
4. A. B. Evlyukhin, S. M. Novikov, U. Zywietz, R. L. Eriksen, C. Reinhardt, S. I. Bozhevolnyi, and B. N. Chichkov, Nano Lett. **12**, 3749 (2012).
5. P. Tonkaev and Yu. Kivshar, JETP Lett. **112**, 615 (2020).
6. A. I. Kuznetsov, A. E. Miroshnichenko, Y. H. Fu, J. Zhang, and B. Luk'yanchuk, Sci. Rep. **2**, 492 (2012).
7. E. Tiguntseva, K. Koshelev, A. Furasova, P. Tonkaev, V. Mikhailovskii, E. V. Ushakova, D. G. Baranov, T. Shegai, A. A. Zakhidov, Y. Kivshar, and S. V. Makarov, ACS Nano **14**, 8149 (2020).
8. N. M. Shubin, V. V. Kapaev, and A. A. Gorbatsevich, JETP Lett. **116**, 205 (2022).
9. A. M. Chernyak, M. G. Barsukova, A. S. Shorokhov, A. I. Musorin, and A. A. Fedyanin, JETP Lett. **111**, 46 (2020).
10. C. W. Hsu, B. Zhen, A. D. Stone, J. D. Joannopoulos, and M. Soljačić, Nat. Rev. Mater. **1**, 16048 (2016).
11. A. B. Evlyukhin, V. R. Tuz, V. S. Volkov, and B. N. Chichkov, Phys. Rev. B **101**, 205415 (2020).
12. A. V. Prokhorov, A. V. Shesterikov, M. Yu. Gubin, V. S. Volkov, and A. B. Evlyukhin, Phys. Rev. B **106**, 035412 (2022).
13. Y. Li, J. Zhang, D. Huang, H. Sun, F. Fan, J. Feng, Z. Wang, and C. Z. Ning, Nat. Nanotechnol. **12**, 987 (2017).
14. G. A. Ermolaev, D. V. Grudinin, Y. V. Stebunov, et al., Nat. Commun. **12**, 854 (2021).
15. M. M. Glazov and E. L. Ivchenko, JETP Lett. **113**, 10 (2021).
16. A. B. Evlyukhin, M. A. Poleva, A. V. Prokhorov, K. V. Baryshnikova, A. E. Miroshnichenko, and B. N. Chichkov, Laser Photon. Rev. **15**, 2100206 (2021).
17. A. B. Evlyukhin, T. Fischer, C. Reinhardt, and B. N. Chichkov, Phys. Rev. B **94**, 205434 (2016).
18. A. B. Evlyukhin and B. N. Chickov, Phys. Rev. B **100**, 125415 (2019).
19. D. Ghazaryan, M. T. Greenaway, Z. Wang, et al., Nat. Electron. **1**, 344 (2018).
20. I. G. Lezama, A. Arora, A. Ubaldini, C. Barreteau, E. Giannini, M. Potemski, and A. F. Morpurgo, Nano Lett. **15**, 2336 (2015).
21. A. R. Beal and H. P. Hughes, J. Phys. C: Solid State Phys. **12**, 881 (1979).
22. A. Baranov and E. Tournie, *Semiconductor Lasers. Fundamentals and Applications,* Vol. 33 of *Woodhead Publishing Series in Electronic and Optical Materials* (Woodhead, Oxford, 2013).
23. Q. Gu and Y. Fainman, *Semiconductor Nanolasers* (Cambridge Univ. Press, Cambridge, 2017).
24. L. Li, M.-F. Lin, X. Zhang, A. Britz, A. Krishnamoorthy, R. Ma, R. K. Kalia, A. Nakano, P. Vashishta, P. Ajayan, M. C. Hoffmann, D. M. Fritz, U. Bergmann, and O. V. Prezhdo, Nano Lett. **19**, 6078 (2019).
25. C. Z. Ning, IEEE J. Sel. Top. Quantum Electron. **19**, 1503604 (2013).
26. B. Munkhbat, P. Wrobel, T. J. Antosiewicz, and T. Shegai, arXiv: 2203.13793 (2022).
27. Z. -Y. Li and Y. Xia, Nano Lett. **10**, 243 (2010).
28. Y. Zhang, J. Li, Y. Wu, L. Liu, X. Ming, T. Jia, and H. Zhang, Plasmonics **12**, 1983 (2017).
29. U. Zywietz, A. B. Evlyukhin, C. Reinhardt, and B. N. Chichkov, Nat. Commun. **5**, 3402 (2014).
30. A. A. Zharov and N. A. Zharova, J. Exp. Theor. Phys. **135**, 808 (2022).

Translated by R. Tyapaev